First cryomodule with Nb_3Sn cavities for beam acceleration test at Jefferson Lab

U. Pudasaini[1], G. Eremeev[2], A. Reilly[1], G. Ciovati[1], J. Fischer[1], M. Drury[1], M. McCaughan[1], R. Rimmer[1], M. Weaks[1], K. Macha[1], C.E. Reece[1], R. Geng[1], S. Wang[1], S. Posen[2], S. Cheban[2], B. Tennis[2]

[1]Thomas Jeferson National Accelerator Facility, Newport News, VA, USA
[2]Fermi National Accelerator Laboratory, Batavia, IL, USA

Abstract

Nb_3Sn with a superconducting transition temperature and superheating field approximately twice that of Nb, is poised to replace Nb to improve the cost and efficiency of SRF accelerator cavities. The successful deployment of Nb_3Sn cavities, capable of delivering performance at 4.4 K comparable to that of Nb cavities at 2 K, would be a significant advancement with the potential to benefit a wide range of SRF accelerator applications. However, this technology has yet to be practically demonstrated in accelerator structures for beam acceleration. A cryomodule was built for the first time with two five-cell Nb cavities coated with Nb_3Sn. During the cryomodule acceptance testing, the cavities reached a maximum accelerating gradient of ~8 MV/m and 13 MV/m with a total dynamic heat load of 75 W at 4.4 K. The cryomodule is planned to be installed and used to accelerate the beam in the upgraded injector test facility (UITF) at Jefferson Lab.

1. Introduction

Accelerator cryomodules are integral to current and future accelerators, providing essential capabilities for high-efficiency particle acceleration. The main component of the modern cryomodules are superconducting radiofrequency (SRF) cavities made of Nb. Nb ($T_c \sim 9.2$ K and $H_{sh} \sim 200$ mT) is the material of choice because of its best superconducting properties (Type II superconductor with the highest T_c and H_{c1}) among all the pure elements. It is easily formable into complex geometries [1]. Even though SRF cavities made of Nb are significantly more economical and efficient than normal conducting copper cavities, optimum performance is often attained at about 2 K. Sophisticated cryogenic facilities based on superfluid liquid helium required to achieve such low temperatures are costly to build, operate, and maintain. After continuous research over the past five decades, the state-of-the-art Nb cavities are approaching performances close to the theoretical best performances defined by the intrinsic material properties [2, 3]. While new processes such as impurity (e.g., N, O) doping or infusion and low/mid temperature treatments are redefining attainable performance limits with Nb [4-6], the desire for ever more energetic, economical, efficient, and simplified particle accelerators inspires the pursuit of alternatives based on better superconducting materials for SRF cavities.

Nb_3Sn promises better performance and a significant reduction of production and operational cost for SRF cavities because both the critical temperature and superheating field

of Nb_3Sn, T_c ~18.2 K and H_{sh} ~400 mT, are nearly twice that of niobium [1]. The superheating field corresponds to a maximum gradient of about 100 MV/m for typically used cavity geometries, almost twice that of Nb. It is currently the front-running alternative material to replace niobium in SRF accelerator cavities. The potential operation of Nb_3Sn-coated SRF cavities at 4.4 K, delivering similar performance to that of Nb cavities at 2 K ($Q_0 > 10^{10}$), has generated significant excitement within the accelerator community. These cavities can be operated with atmospheric liquid helium or cryocoolers, simplifying and reducing the cost of cryogenic facilities. The successful deployment of Nb_3Sn cavities could be a transformational technology that will benefit numerous SRF accelerator applications. Despite early interest in the 1970s, the development of Nb_3Sn-coated cavities was halted due to a persistent Q-slope issue that was thought to be a fundamental problem [7, 8]. In contrast, performance improvements in Nb cavities progressed rapidly. Over the past 15 years, resumed research efforts have significantly improved the Nb_3Sn cavity performance. Compared to the attainable maximum gradient with $Q_0 > 10^{10}$ at 4.4 K, starting at about 6 MV/m in the 1990s and ~13 MV/m in 2014, 1.3 GHz single-cell cavity attaining ~18 MV/m was demonstrated in different labs [9-13]. The record performance was achieved in a 1.3 GHz cavity coated at Fermilab that achieved 23 MV/m with $Q_0 \sim 10^{10}$ at 4 K [13]. Significant progress has been made with multi-cell cavities such as CEBAF 5-cell and ILC type 9-cell cavities, attaining an accelerating gradient of ~15 MV/m [13, 14]. There have been successful tests of Nb_3Sn cavities operating in conduction-cooled setups as needed for the development of accelerators for industrial or environmental remediation at Fermilab (650 MHz single cell cavity), JLab (1.5 GHz and 952 MHz single cell), and Cornell (2.6 GHz) [15-18]. Detailed plans have been published for a medium-energy, high average-power superconducting e-beam accelerator by researchers at Fermilab [19] and a cw, low-energy, high-power superconducting linac by researchers at JLab [20]. Until recently, there have been only a few instances of constructing cryomodules with Nb_3Sn-coated cavities, and none had been used for beam acceleration—except for a conduction-cooled Nb_3Sn cryomodule with a 650 MHz five-cell cavity, developed recently in China [21].

Before the recent upgrade of the booster cryomodule [22], the injector section of CEBAF used a standalone cryomodule comprising two hermetically sealed 1.5 GHz 5-cell niobium cavities. Such a cryomodule, operated for over three decades, is essentially a quarter of a standard CEBAF cryomodule used in the main linacs, as shown in Figure 1 [23]. A cryostat and other hardware components from a spare injector cryomodule and two new Nb_3Sn-coated cavities were used to develop the first Nb_3Sn quarter cryomodule with the aim of a beam test. C75-style cavities, instead of C20 cavities, were used, aiming for a 10 MeV cryomodule that could be used at the Upgraded Injector Test Facility (UITF) at Jefferson Lab for beam acceleration. This tech note will discuss the fabrication of the Nb_3Sn cavities, assembly of the cryomodule, results from the acceptance test of the module, and plan for the beam test.

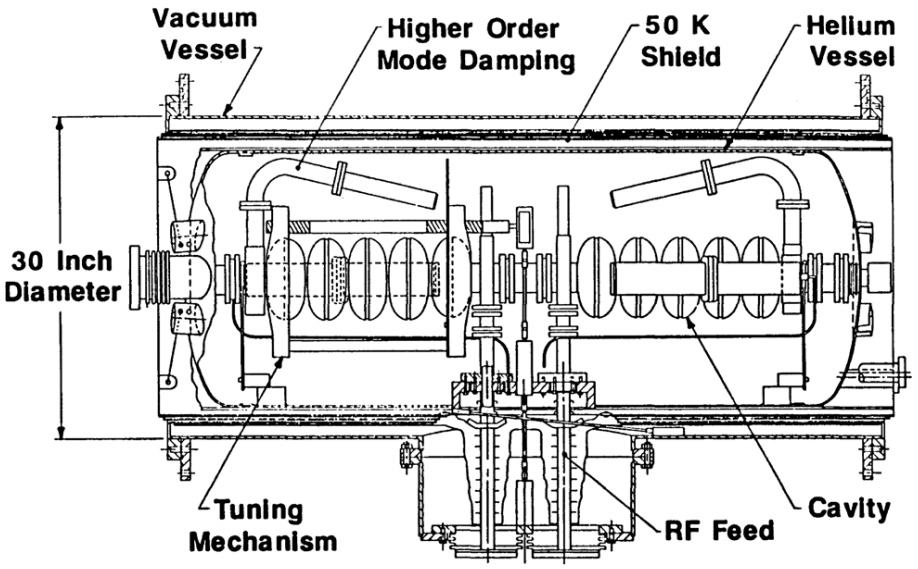

Figure 1: Schematic diagram of a CEBAF quarter cryomodule consisting of two five-cell 1497MHz cavities.

2. Cavity qualification

Two Nb cavities, 5C75-RI-NbSn01 and 5C75-RI-04, built by RI Research Instruments, GmbH, according to Jefferson Lab's specifications, were used as the substrate to grow Nb_3Sn coating inside each cavity. 5C75-RI-NbSn01 cavity cells were made of high-purity (RRR>300), fine-grain material, and 5C75-RI-04 cavity cells were made of large-grain Nb material with RRR = 200. The cavities were electropolished for 100 - 120 μm of bulk removal, annealed in a vacuum at 800 °C for 2 - 3 hours to degas hydrogen, and received final electropolishing for 25 - 30 μm to refresh the surface after annealing. In the baseline test, 5C75-RI-NbSn01 reached $E_{acc} \sim 29$ MV/m with a low-field Q_0 of about 2×10^{10} at 2.0 K. 5C75-RI-04 was limited to ~18 MV/m by multipacting-induced quench with the low-field Q_0 of $\sim 1.2 \times 10^{10}$ at 2.07 K.

5C75-RI-NbSn01 was first coated with Nb_3Sn at Jefferson Lab and assembled into a pair with 5C75-RI-NbSn02, a similar cavity also coated at Jefferson Lab [24]. As reported in [25], performance degradation was observed during the vertical testing of the cavity pair, likely stemming from mechanical stress on the coated cavities, which required reprocessing and recoating cavities with Nb_3Sn to qualify the cavities for the cryomodule. 5C75-RI-NbSn01 was then transferred to Fermilab for reprocessing and Nb_3Sn coating deposition. While processing the second cavity, 5C75-RI-NbSn02 developed a vacuum leak in a weld joint of the fundamental power coupler end group, resulting in a replacement with 5C75-RI-04, as mentioned above, for coating at Jefferson Lab. Both cavities were tuned to a frequency of

1493.7±0.1 MHz at room temperature to avoid mechanical tuning after the coating and ensure a field flatness >90%.

2.1 5C75-RI-04 cavity coating and qualification at Jefferson Lab

Following the baseline test, the 5C75-RI-04 cavity received HPR before the assembly for the coating in the cleanroom. Three Sn and $SnCl_2$ sources were used: the first at the bottom (3.76 g of Sn and 2 g of $SnCl_2$), the second around the center (1.05 g of Sn and 0.5 g of $SnCl_2$), and the third close to the top of the cavity (0.82 g of Sn and 0.5 g of $SnCl_2$) to ensure uniform coating growth conformably. The amount of Sn consumed was 3.64 g, 0.9 g, and 0.6 g from the crucibles at the bottom, center, and top, respectively. The coating process was adjusted based on the experience of the coating process for five-cell cavity cavities [24]. The temperature profile consists of ~12 h of baking at ~ 120 °C followed by a 5 h nucleation step at 500 °C and 5.8 h of coating at 1200 °C, as shown in Figure 2. At the end of the process, the heat was turned off, and the setup was vacuum-cooled to room temperature.

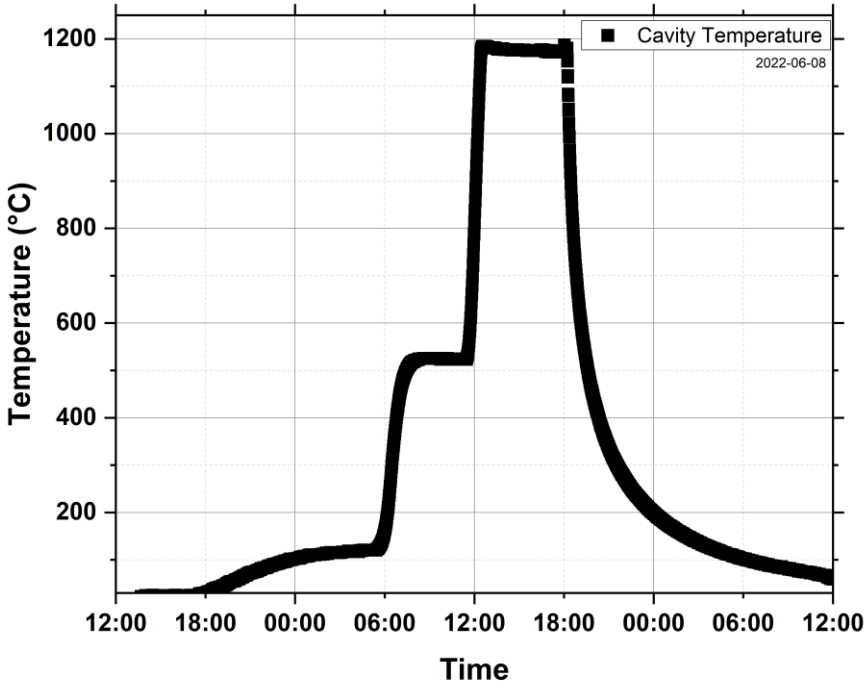

Figure 2: Temperature Profile used to coat 5C75-RI-04 cavity at Jefferson Lab. Note that the cavity temperature was measured using a Type C thermocouple touching the cavity surface.

During the visual inspection, the cavity was found to be coated uniformly, as shown in Figure 2. No uniformity asymmetry was observed from different ends of the cavity. The witness samples, installed inside the cavity before the coating, were analyzed with scanning electron microscopy (SEM) equipped with energy dispersive X-ray spectroscopy (EDS), and

atomic force microscopy (AFM) also revealed uniform coating. A typical coating microstructure on the witness sample is shown in the AFM image, Figure 3.

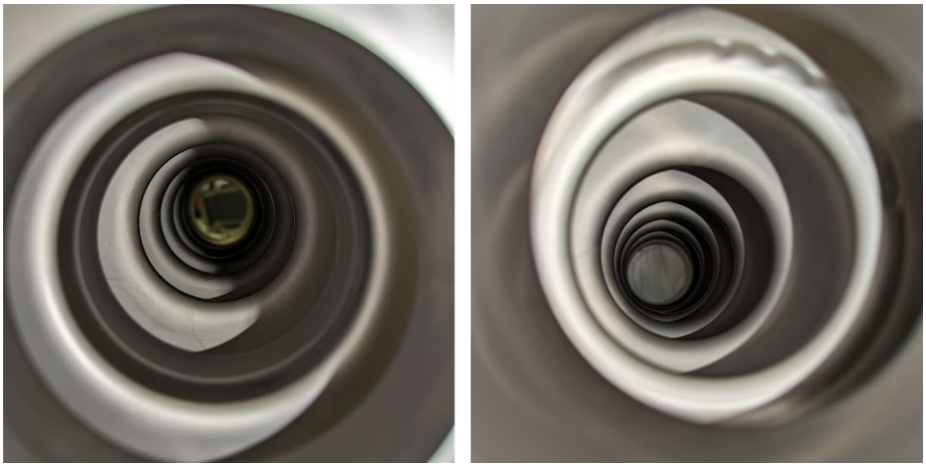

Figure 2: The interior surface of the 5C75-RI-04 cavity after Nb_3Sn coating from the top [left] and bottom [right]. The cavity looked uniformly coated from each end and other ports.

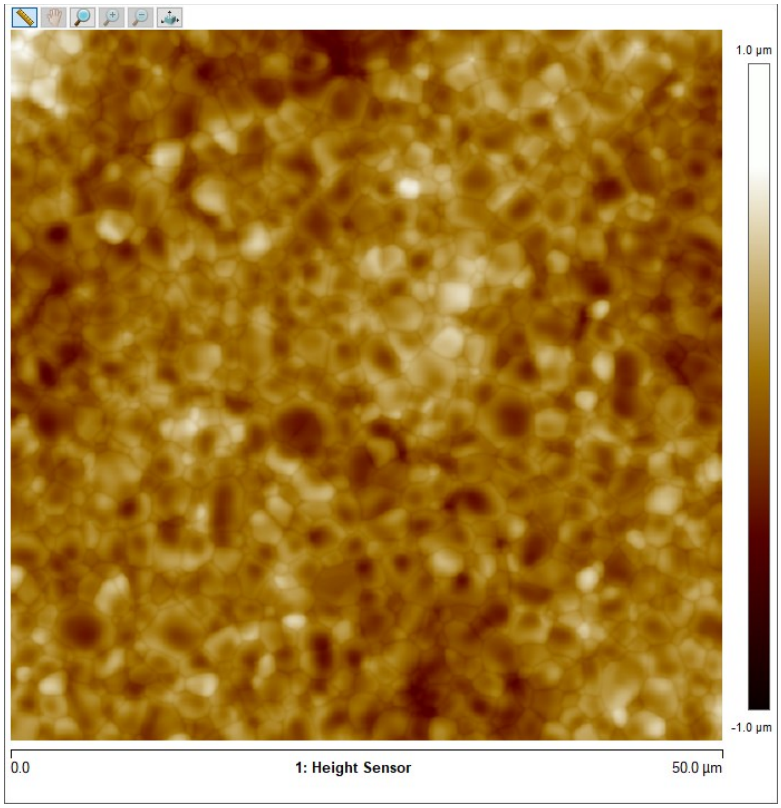

Figure 3: AFM image from the witness sample coated with 5C75-RI-004. The average roughness (R_a) was 120 nm.

The cavity followed the typical procedures for testing the Nb SRF cavity after the coating. The cavity was ultrasonically degreased with 1-2% Liquinox, then high-pressure

rinsed with DI water before assembly in the clean room for RF testing. The assembled cavity was then slowly pumped down before being loaded into the dewar for testing at cryogenic temperatures. The dewar was then cooled with liquid helium to about 4.4 K. The dewar was then slowly warmed to approximately 19 K, and the temperature was slowly lowered using controls provided by the JT helium supply valve and heater power at the bottom of the dewar for uniform cooldown. The temperature gradient across the cavity was maintained at about ~0.1 K while cooling down through the transition temperature between 17.5 K and 18.5 K. RF test results at 4.4 K and 2 K are shown in Figure 4. The cavity quality factor was about 2×10^{10} at the low field and maintained above 10^{10} at 10 MV/m at 4.4 K. The performance was measured up to 13.3 MV/m before a multipacting barrier limited the test. More RF power was not used to process the multipacting to avoid any potential degradation of the cavity performance. No radiation was observed during the test. The low-field quality factor was above 3×10^{10} at 2 K and possessed characteristics similar to those of the cavity at 4.4 K, except for a higher quality factor. The quality factor at 2 K is believed to be influenced by higher residual resistance, and it is likely that surface Sn residues, similar to those observed in the witness sample, may have contributed to this.

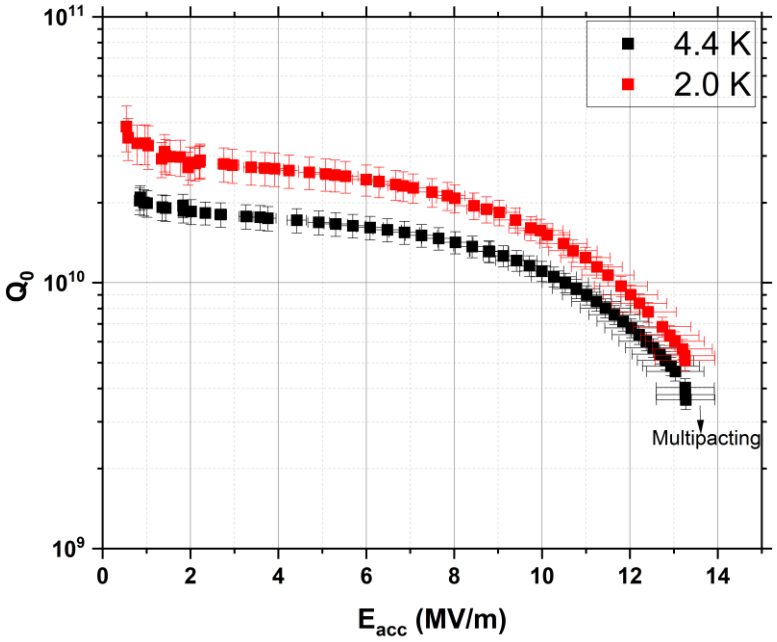

Figure 4: Performance of 5C75-RI-04 cavity after Nb_3Sn coating at 4.4 K (black) and 2.0 K (red). 4.4 K (bottom).

2.2 5C75-RI-NbSn01 cavity coating and qualification Fermilab

5C75-RI-NbSn01 cavity received 35 μm of electropolishing in the Argonne National Laboratory facility to reset the Nb_3Sn-coated surface for the new coating. The complete cavity

was then anodized by applying a voltage of 30 V in a 0.1 M diluted sulfuric acid solution as a part of the coating protocol followed in Fermilab. Each end of the cavity had a crucible installed with the required amounts of Sn and $SnCl_2$. Both crucibles were equipped with heaters to control the temperature individually. The coating setup and procedure were similar to the one used for several multi-cell cavities coated before [13], but this was the first time a C75-shaped five-cell cavity was coated in this facility. The temperature profile used to coat this cavity was similar to one reported in [13], see Figure 5, with some modifications. The cavity coating process was initiated after degassing the cavity for 23 h at 140 °C. The coating process includes a modified nucleation step, which includes a fast ramp of Sn and $SnCl_2$ crucibles to 700 °C and soaking for 1 hour, then keeping the temperature constant at 500 °C for 4.5 h. The furnace temperature was then raised to 1100 °C while maintaining the Sn source 200°C hotter than the furnace for 3 hours. The final step was annealing at 1100 °C for 3 hours. The cavity was visually observed to be uniformly coated and shiny compared to another cavity coated at Jefferson Lab, as shown in Figure 6. The witness sample coated with the cavity was examined using SEM/EDS and AFM. A uniform coating was observed, and Nb_3Sn grains were smaller than JLab-coated samples, as shown in the AFM image, Figure 7.

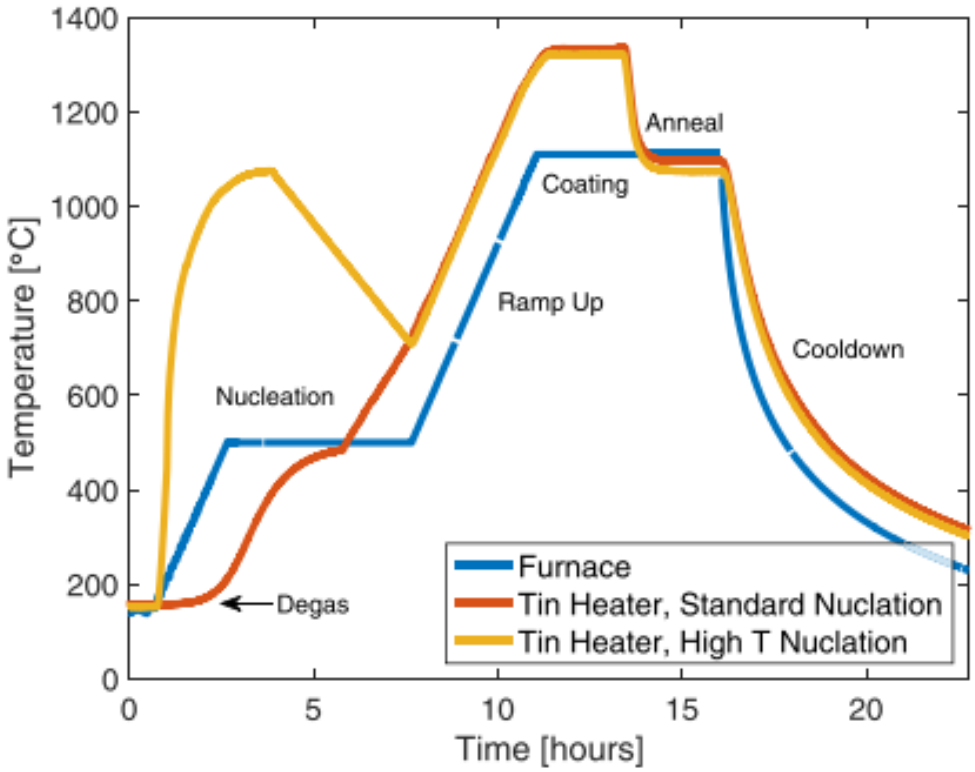

Figure 5: Typical temperature profile for Nb_3Sn coating of Nb cavity at Fermilab. Note that the coating durations were adjusted to coat 5C75-RI-NbSn01

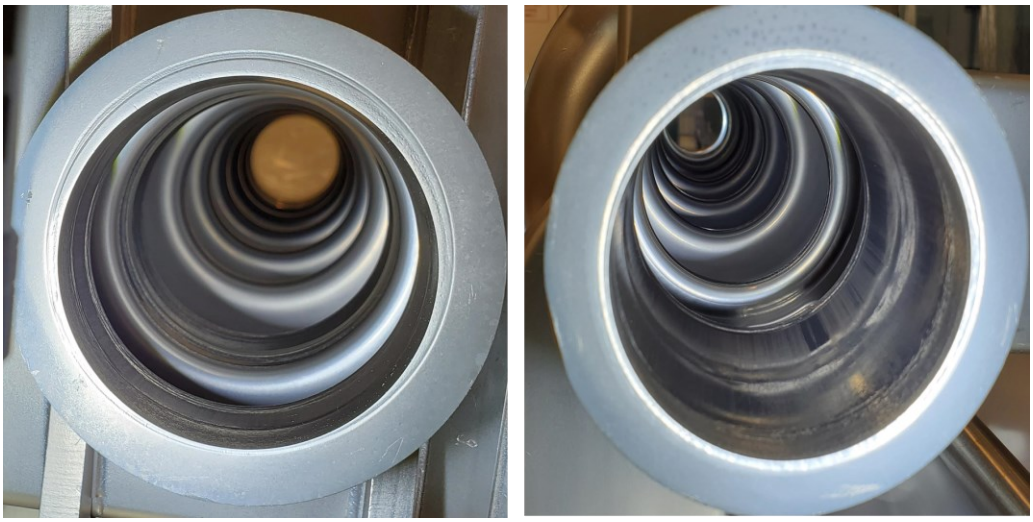

Figure 6: Appearance of the interior surface of the 5C75-RI-0NbSn01 cavity after Nb_3Sn coating from the front end (FPC side) [left] and rare end [right]. The cavity looked glossy and uniformly coated inside.

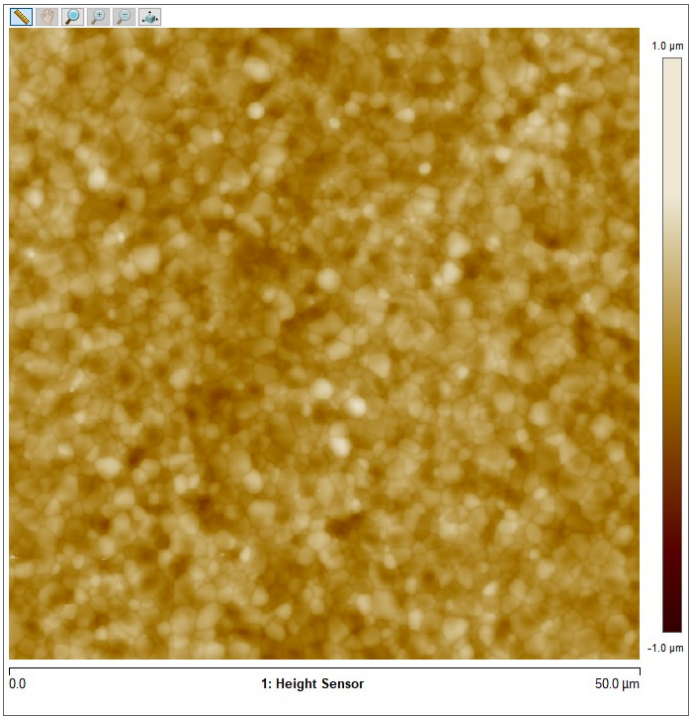

Figure 7: AFM image from the witness sample coated with 5C75-RI-NbSn01 at Fermilab. The average roughness (R_a) was 80 nm.

The performance of the coated 5C75-RI-NbSn01 was evaluated in a vertical test cryostat using typical cavity RF measurement procedures at Fermilab. The post-coating cleaning and assembly steps followed for the RF test were similar to those described for the 5C75-RI-04 cavity at Jefferson Lab. The cavity was cooled slowly and uniformly through the

critical temperature of ~18 K to prevent performance degradation due to the trapped magnetic field produced by thermo-currents. RF tests were performed at 4.4 K with liquid helium and superfluid helium at ~2 K. Figure 8 summarizes the test results from each temperature. The cavity's quality factor was above 10^{10} in the low field and maintained close to 10^{10} at 10 MV/m at 4.4 K. The performance was limited to ~14 MV/m by multipacting-induced quench where the quality factor was 6×10^{9}. Radiation was not observed during RF tests. The low-field quality factor was above 4×10^{10} at 2 K and possessed characteristics similar to those of the cavity at 4.4 K, except for a higher quality factor. Since both cavities demonstrated suitable performance for the quarter cryomodule to be installed in the UITF, they progressed with a pair assembly to build the cryomodule.

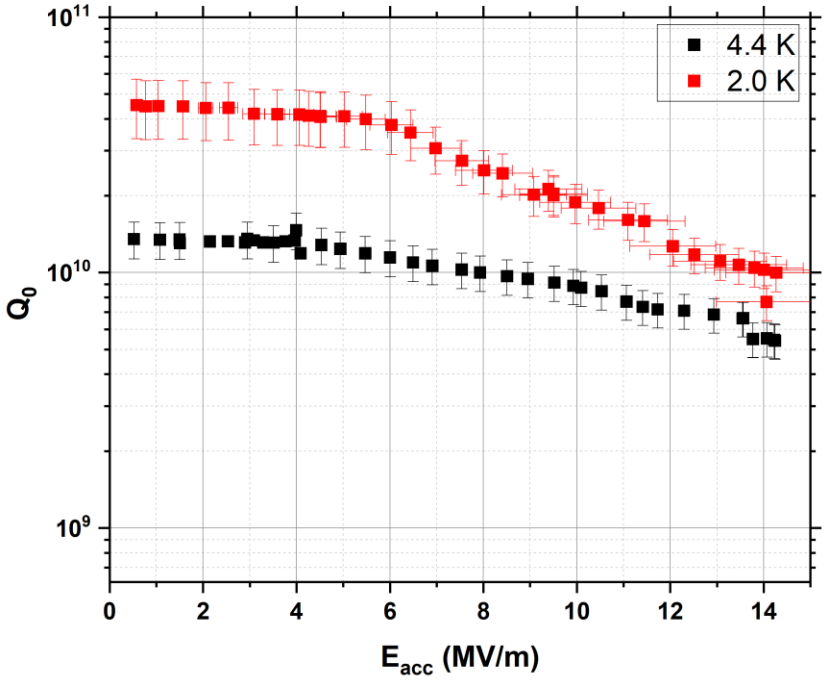

Figure 8: Performance of 5C75-RI-NbSn01cavity after Nb_3Sn coating at 4.4 K (black) and 2 K (red) at Fermilab

3. Cryomodule Assembly

The usual step of tuning cavities to a frequency was eliminated to avoid performance degradation from mechanical stress [25]. Note that each cavity was tuned before the coating to bring the frequency of coated cavities close to the target frequency. The beamline and waveguide flange sealing surfaces were carefully polished, and special plugs were installed into waveguides to prevent chemical vapor from reaching the coated cavity surface while applying light chemical treatment to the flanges' surface before the pair assembly. A dog-leg

waveguide with a ceramic RF window on the FPC port and Nb elbows on both HOM waveguide ports was assembled, as shown in Figure 9. The two cavities were connected with an adapter. After the pair assembly was completed, a vacuum leak was detected in the ceramic window attached to the fundamental power coupler of the 5C75-RI-04 cavity. Since replacing the window could introduce particles inside the cavity pair, which would likely result in performance degradation due to field emission, the pair required complete disassembly, recleaning, and careful reassembly. Since the disassembly of the pair poses the risk of mechanical stress on the cavity, potentially causing performance degradation, each cavity was tested individually in the vertical dewar again.

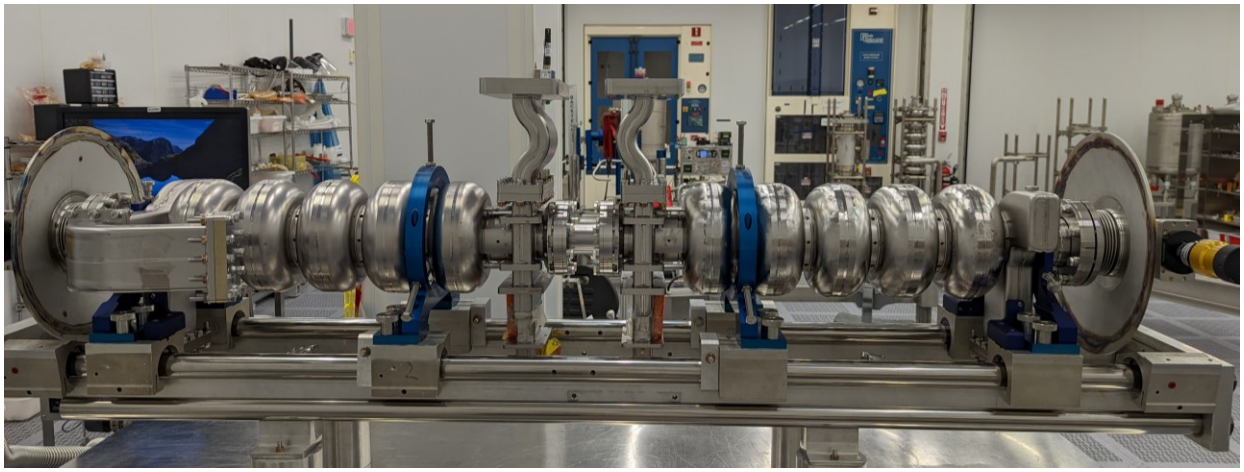

Figure 9: Cavity pair assembled with 5C75-RI-NbSn01 (left) and 5C75-RI-04 (right).

Following the pair disassembly, each cavity followed the typical processing steps for RF testing. It was discovered that the 5C75-RI-04 cavity performance was degraded compared to the pre-pair assembly into the pair. Despite the low field quality factor of $>10^{10}$ at a low field at 4.4 K, a sharp drop in quality factor was observed starting at 3 MV/m. The cavity was quench limited to ~ 8.2 MV/m with no radiation, as shown in Figure 10.

The other cavity, 5C75-RI-NbSn01, did not show any noticeable degradation following the pair disassembly. The cavity reached ~20 MV/m at 2 K, potentially because of the successful processing of multipacting at Jefferson Lab. Since the average accelerating gradient of the two cavities was still above 10 MV/m, they were progressed for the pair assembly again. Additional precautions were taken while applying torque to the flanges during the assembly to minimize the mechanical strain on the cavity. No leak was discovered during the leak check this time. Typically, the pair is subjected to final cryogenic testing in a vertical dewar to check for any performance degradation and potential cryogenic leaks. Since Nb_3Sn cavity pair testing has resulted in performance degradation in the past because of mechanical stress in the cavity while linked to hanging vertically and crane movement, which was corroborated by mechanical simulations [25], this step was eliminated before installing it into the helium vessel.

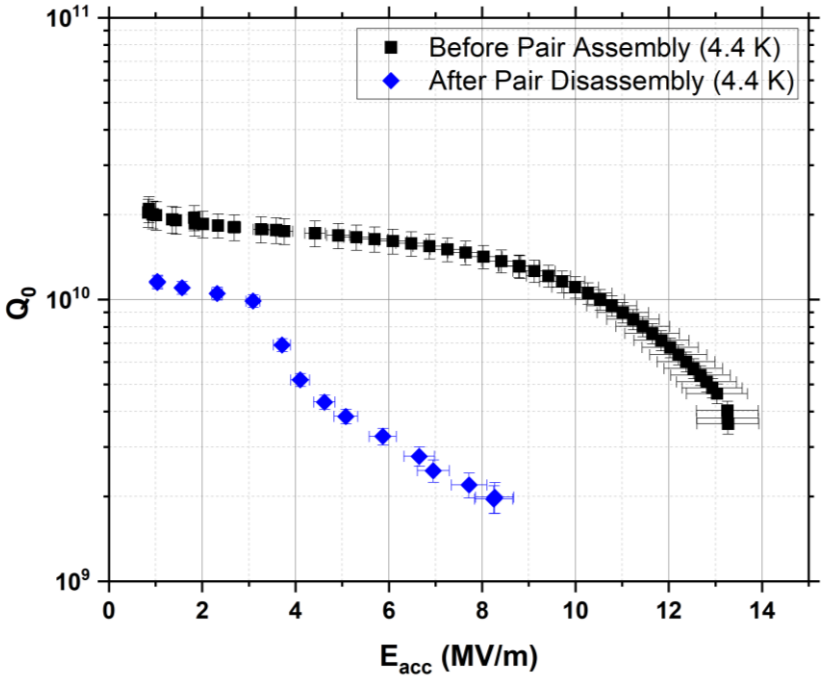

Figure 10: Performance of 5C75-RI-04 during the individual cavity test before (black) and after (red) at 4.4 K.

Two Cernox™ sensors, one each near the beamline flange at the end of each cavity, were installed to monitor the temperature gradient across the cavity pair during the cryomodule cooldown, as shown in Figure 11. The distance between the two temperature sensors is ~140 cm. Additionally, two flux gate magnetometers, one to the second cell of the first cavity and another to the fourth cell of the second cavity, each positioned at a 45° angle relative to the cavity pair axis, see Figure 12, were epoxied to monitor the ambient magnetic field. Silicon diodes are also installed on midplane of the HOM elbows of each cavities. The cryomodule assembly steps involved attaching the cold tuner and cavity magnetic shield, welding the stainless-steel helium vessel to the end dishes, and finally sliding the assembly into the cryogenic vacuum vessel. Tuner cell holders were installed without shims to eliminate any pressure on the cell during cooldown. In addition, no pre-loading was done with the tuner. A special torque procedure was employed to avoid bending the pair while attaching the FPC flanges to the vacuum vessel: starting with a 0.125" shim, the pair was slowly raised, and the gap between the flange and the helium vessel was checked regularly. The process was repeated with a 0.060" shim to ensure equal space around the sealing surfaces. Dial indicators were mounted to ensure even tightening while the indium seal was torqued. The center frequency for the tuner range was set to 1496.1 MHz for both cavities, and the tuner range interlock was spread out to increase the tuner range. The vacuum level inside the pair was regularly monitored for potential leaks, and the cavities' frequency was tracked throughout the assembly steps, as summarized in Table 1; after completing all the

assembly steps, the frequency shift was approximately -170 kHz for 5C75-RI-NbSn1 and 20 kHz for 5C75-RI-04. Beginning with the assembled cavity pair, Figure 13 summarizes the evolution of the cryomodule assembly up to the point it was installed in the Cryomodule Test Facility (CMTF).

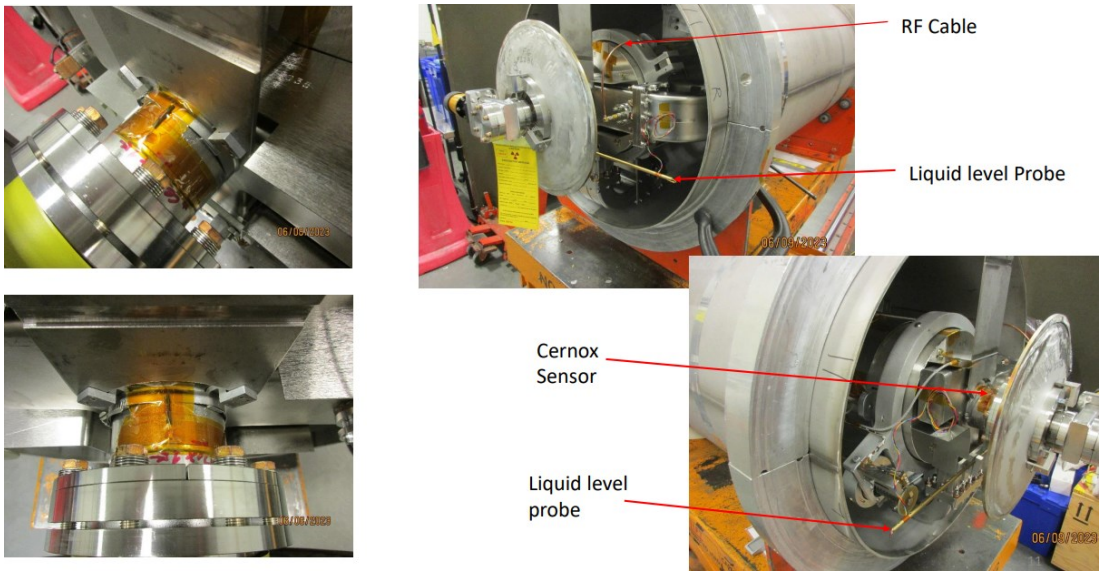

Figure 11: Position of Cernox sensors attached to each cavity. Note that the temperature difference measured by these sensors represents the temperature gradient across the cavity pair.

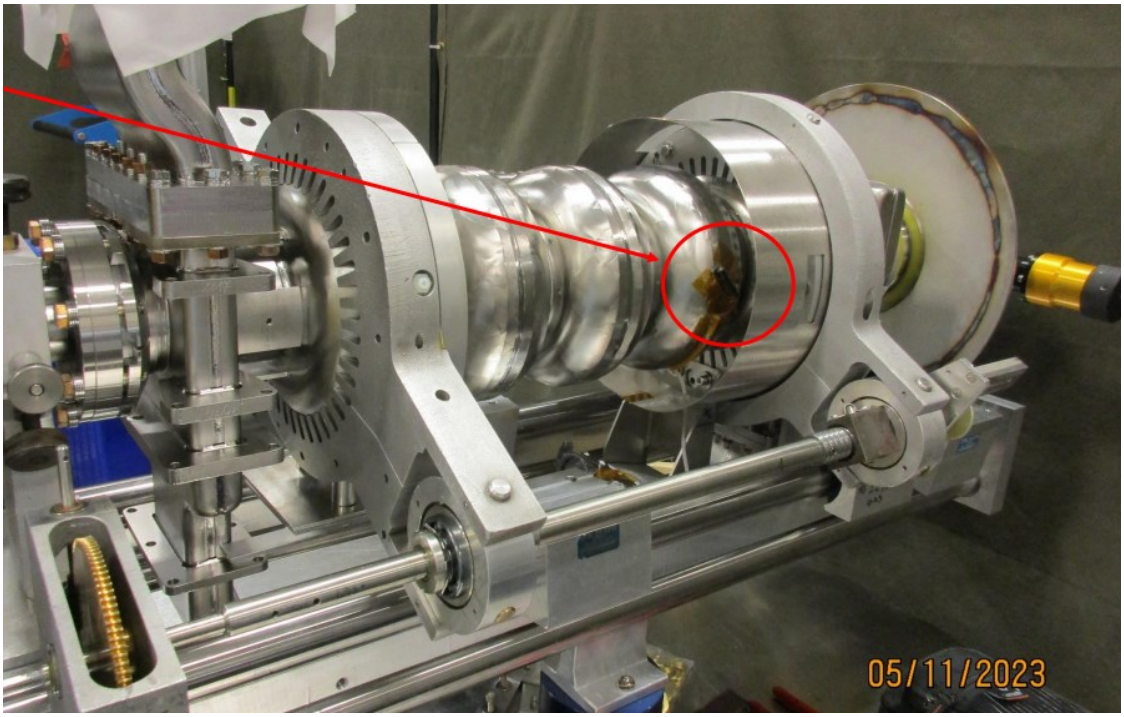

Figure 12: Position of flux gate magnetometers, as indicated by the red arrow epoxied to the fourth cell of the cavity at an angle of 45° relative to the cavity axis.

Table 1: The cavity π-mode frequency recorded at key cryomodule assembly steps.

Assembly step	5C75-RI-NbSn01 (MHz)	Frequency change from assembly step (MHz)	5C75-RI-004 (MHz)	Frequency change from assembly step (MHz)	Frequency difference between two cavities (MHz)
Post CMM	1494.342		1494.002		0.340
Post Tuner Install	1494.338	-0.004	1493.984	-0.018	0.354
Pre-HV Install	1494.300	-0.038	1493.995	0.011	0.305
Post-HV Install	1494.295	-0.005	1493.985	-0.01	0.310
Post-Fixture Removal	1494.270	-0.025	1494.005	0.02	0.265
Pre HV evac	1494.135	-0.135	1493.945	-0.06	0.190
Post HV evac	1494.120	-0.015	1493.920	-0.025	0.200
Post Waveguide	1494.135	0.015	1493.940	0.02	0.195
Post move to 2nd	1494.135	0	1493.945	0.005	0.190
Post Bridging Ring	1494.090	-0.045	1493.945	0	0.145
Pre-Ins Vac	1494.117	0.027	1493.922	-0.023	0.195
Post Ins Vac	1494.190	0.073	1494.020	0.098	0.170
Post Pressure test	1494.174	-0.016	1494.024	0.004	0.150

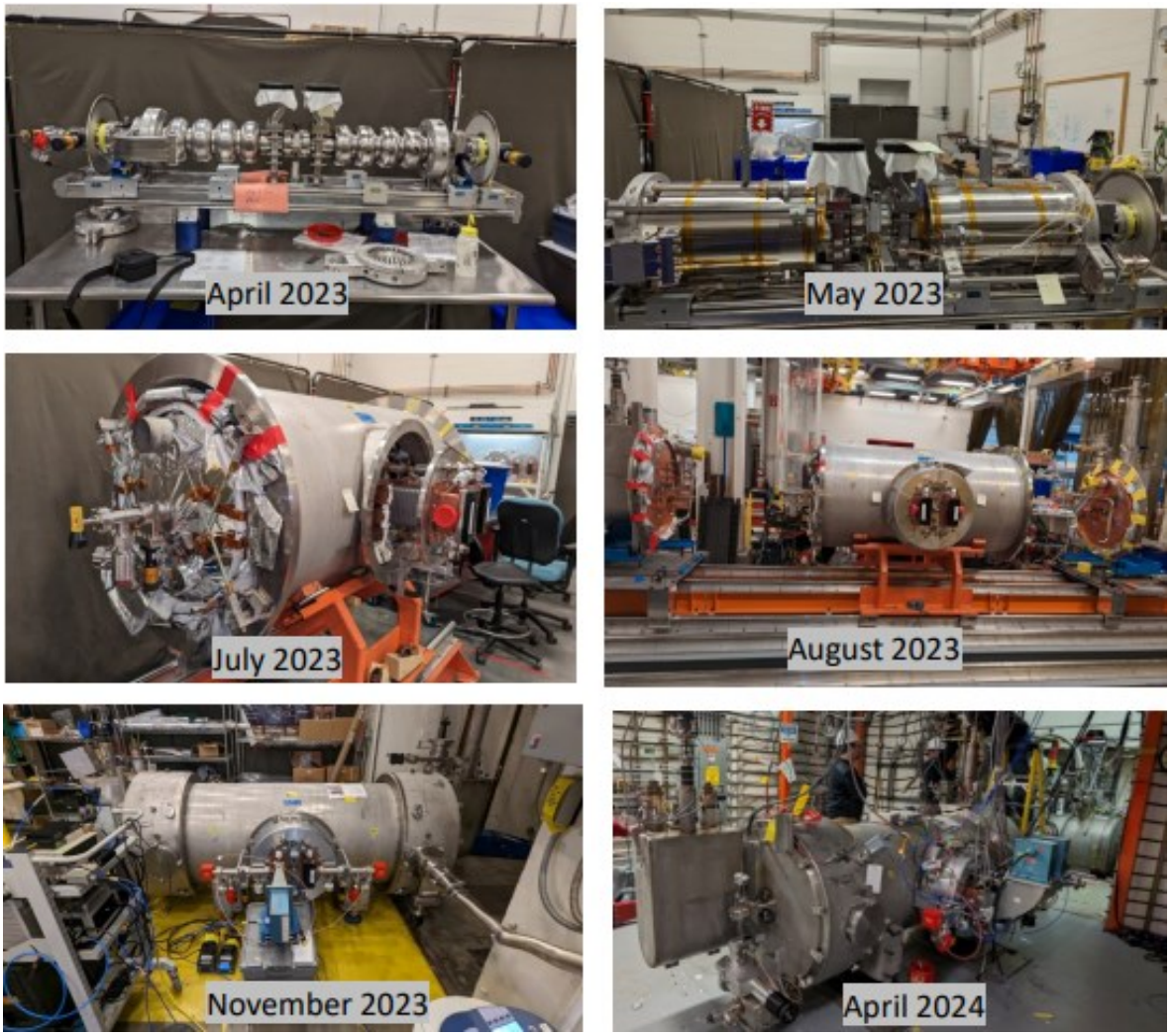

Figure 13: Different stages of cryomodule assembly, from the assembled pair to the installed cryomodule in the CMTF.

4. Cryomodule Testing

The cooldown procedure for the cryomodule followed a similar approach to other CEBAF cryomodules, with adjustments made to achieve a cooldown rate of less than 30 K per hour during the initial transition from room temperature to 4.4 K to avoid sudden mechanical stress induced by the cooldown. The residual magnetic field, as measured by the flux gates, was below 10 mG in each cavity. The temperature difference across the length of the cavity pair, monitored by the two Cernox sensors attached to the outer flange of the two cavities, was aimed to be kept below 0.3 K using controls that adjusted the heater power in the liquid helium inlet and the JT valve opening. Note that the temperature gradient across the cavity results in quality factor degradation because of the thermo-current generated by the Nb_3Sn-Nb bimetallic material of the cavity. Temperature measurements were taken using silicon

diodes placed on the HOM elbows inside the helium vessel. The frequency of each cavity was continuously monitored, see Figure 14. The tuner was physically checked during the cooldown to ensure it would not engage, preventing any potential mechanical deformation. Despite the effort in controlling the temperature uniformity over the length of the cavity pair, temperature fluctuations prevented the target temperature difference of 0.3 K from being achieved. The temperature difference measured by Cernox sensors was ~ 0.5 K.

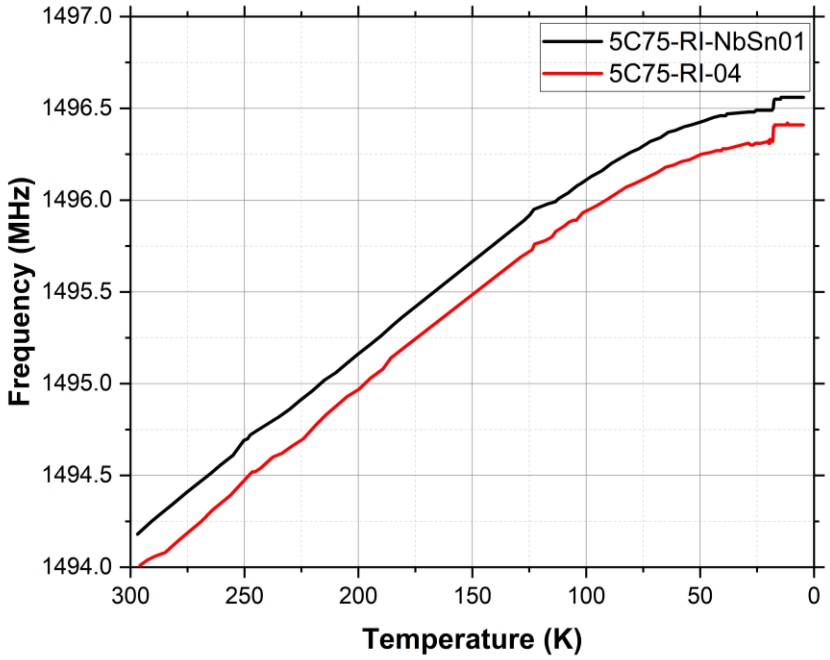

Figure 14: Cavity frequencies during the cryomodule cool-down. Temperatures were measured with diodes attached to the HOM elbow of each cavity.

Following the cooldown, the maximum attainable accelerating gradient, E_{max}, was measured by incrementally raising the RF power. The operational accelerating gradient,"E_{op}," is defined as the highest E_{acc} value at which the cavity can operate stably for at least one hour. The measured E_{max} for 5C75-RI-NbSn01 and 5C75-RI-004 were 13.3 MV/m and 7.9 MV/m, respectively, closely matching their maximum gradients measured in the vertical dewar before the final pair assembly, which were 13.6 MV/m and 7.9 MV/m, respectively. The operational accelerating gradients, E_{op}, were 12.6 MV/m and 7.5 MV/m, respectively. Since each cavity is 0.5 m long, these results demonstrate that the attainable gradients were preserved throughout the cryomodule assembly, and, more importantly, the milestone of achieving a 10 MeV cryomodule was successfully met. A few quenches with radiation were observed during the gradient measurement, but no sustained radiation was observed during the test. The cryomodule was warmed to above 30 K and attempted to cool down uniformly through the transition temperature to release the trapped magnetic flux for the quality factor measurements. Figure 15 shows the temperature gradient across the cavity pair measured

by the Cernox sensors and diodes attached to each cavity while transitioning through the critical temperature. The temperature gradient fluctuations were observed near the transition temperature where the gradient measured by Cernox sensors seemed higher than 0.3 K. The quality factors for each cavity were determined by dLL/dt, the rate of change of the He liquid level. The rate of change was first calibrated using the dissipated power from the electric heater installed in the helium vessel between a known electric heat and the RF heat when a cavity is at a specific gradient at 4.4 K. Figure 16 presents the estimated quality factor as a function of the accelerating gradient. The quality factor measurement, not shown here, was also attempted with flow meter based technique. The reason for the large discrepancy in Q_0 values measured with the dLL/dt method and the flow meter method is not yet understood fully and requires further investigation. Each cavity's measured quality factor was lower than before the cryomodule assembly. The quality factor of the 5C75-RI-NbSn01 cavity decreased approximately by an order of magnitude, while the reduction was less severe in 5C75-RI-04, see Figure 4. Still, the quality factor is notably higher than the Nb cavity at the same temperature. The fluctuations in the inlet temperature of liquid helium around the transition temperature could have caused the temperature gradient fluctuation across the cavity pair leading to low quality factors. The temperature difference across the cavity was higher than those obtained in the vertical test in the dewar, as observed in Figure 15.

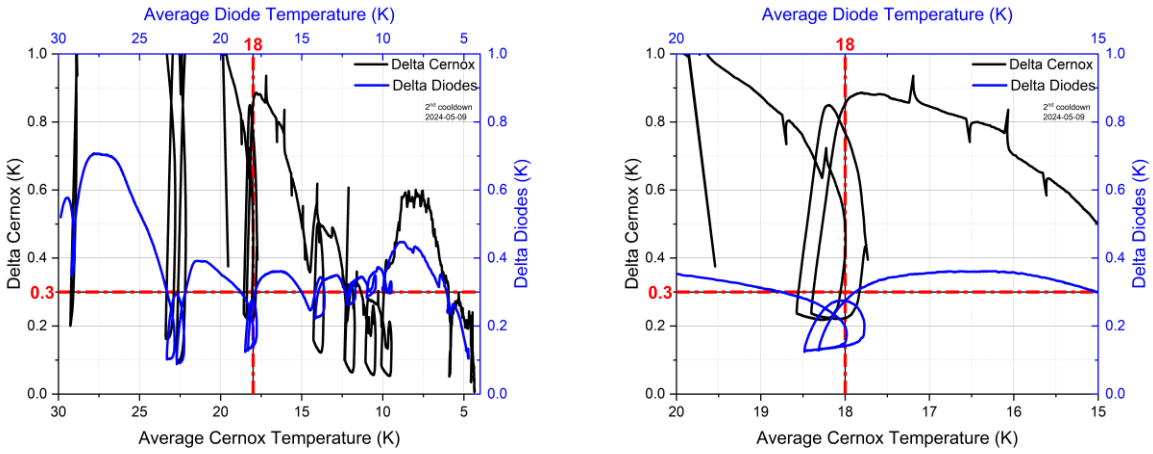

Figure 15: Temperature difference across the cavity pair, measured by Cernox sensors attached to each cavity during thermal cycling from 30 K down to 4.4 K (left). A zoomed-in version shows temperature variation around the superconducting transition temperature (right).

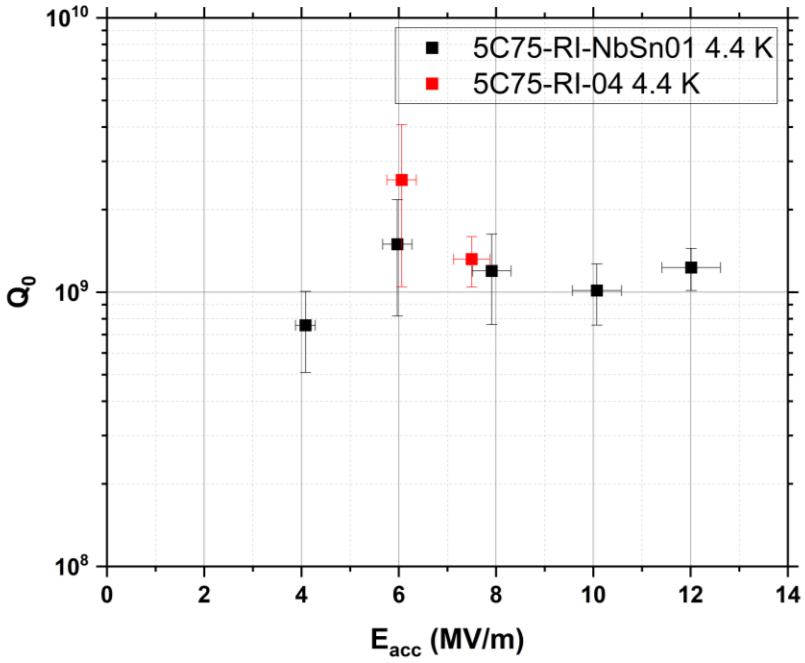

Figure 16: Cavity performance during the cryomodule testing at 4.4 K. The Q_0-values reported are measured with the dLL/dt method.

Following the quality factor measurement at 4.4 K, the cryomodule was pumped down to 2.07 K for E_{max} and E_{op} measurements. The measured E_{max} for 5C75-RI-NbSn01 and 5C75-RI-04 at 2 K were 13.2 MV/m and 8.7 MV/m, respectively, close to those at 4.4 K. The operational accelerating gradients, E_{op}, were 12.4 MV/m and 8.5 MV/m, respectively. Table 2 summarizes the maximum and operational gradients reached for each cavity at 4.4 K and 2.07 K.

Table 2: Maximum and operational gradient measured for each cavity during the cryomodule testing

Cavity	**E_{max} at 4.4 K (MV/m)**	**E_{op} at 4.4 K (MV/m)**	**E_{max} at 2.07 K (MV/m)**	**E_{op} at 2.07 K (MV/m)**
5C75-RI-NbSn01 (cavity #7)	13.3	12.6	13.2	12.4
5C75-RI-04 (cavity #8)	7.9	7.5	8.7	8.5

The cryomodule was slowly warmed to ~30 K and cooled down to ~2.0 K for quality factor measurement. The cooldown was qualitatively more uniform compared to the previous thermal cycle, but the temperature fluctuations were observed, as shown in Figure

17. The horizontal axis is the average of the temperature measure by temperature diodes attached to each cavity. Figure 18 shows the values of Q_0 as a function of the accelerating gradient using the standard method of measuring the rate of rise of the helium pressure. The quality factors were close to 10^{10} at the low field and showed a field dependence similar to those observed during the cavity qualification tests in the vertical dewar. The quality factor values were below those measured at the same temperature before the pair assembly. Since the maximum gradient was similar, we speculate that different cool-down conditions caused the lower quality factor during the cryomodule cool-down compared to the cavity testing in the dewar.

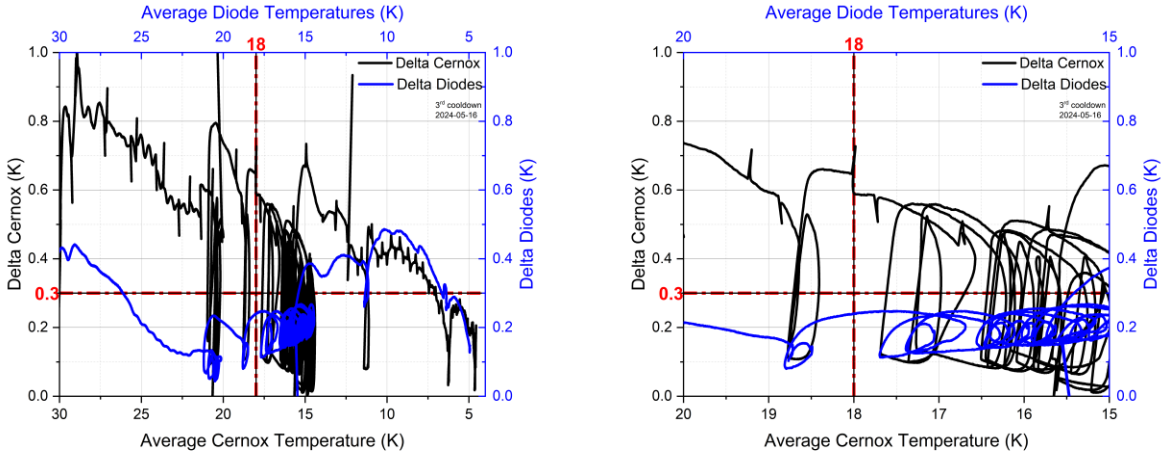

Figure 17: Temperature difference across the cavity pair, measured by Cernox sensors attached to each cavity during thermal cycling from 30 K down to 4.4 K (left). A zoomed-in version shows temperature variation around the superconducting transition temperature (right).

Following the quality factor measurement, the cavity 5C75-RI-04 was tuned ~ 180 KHz to match the frequency of the other cavity and verified that there was no degradation in the maximum attainable gradient, as shown in Figure 18. Table 3 summarizes the measured frequencies of each cavity at different temperatures and shows the post-tuned final frequency. The cryomodule was again warmed up to ~30 K and cooled down to 2.0 K to measure the quality factors following the tuning of the cavity. It was found that there was no notable change in the performance of each cavity, which is consistent with previous results in the vertical dewar testing, where a single cell cavity was tuned [26]. The cavity was detuned to its original frequency before the warm-up to room temperature.

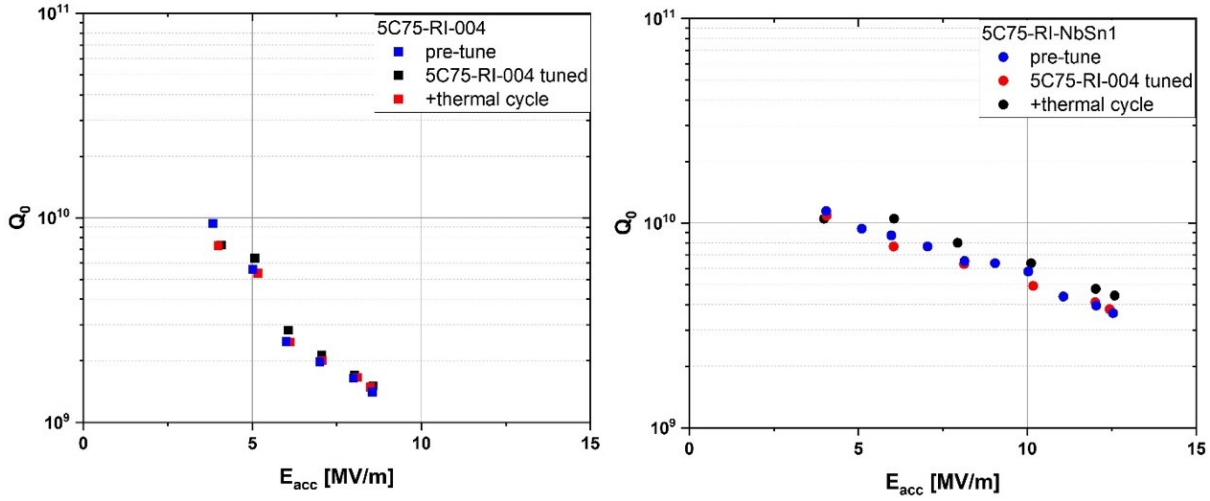

Figure 18: Performance of 5C75-RI-04 [left] and 5C75-RI-NbSn01 Cavity [right] at 2 K.

Table 3: Cavity frequency at different temperatures. Note the frequency of 5C75-RI-04 before and after tuning at 2.1 K.

Cavity	Frequency at 4.4 K (MHz)	Frequency at 2.1 K (MHz)	Post Tuning Frequency at 2.1 K (MHz)
5C75-RI-NbSn01 (cavity #7)	1496.55	1496.59	
5C75-RI-04 (cavity #8)	1496.41	1496.44	1496.61

5. Expected energy gain and beam acceleration at 4.4 K

In the current UITF setup, a 780 nm wavelength laser strikes the photocathode inside the electron gun, causing it to emit electrons. The DC gun's electric field then accelerates these electrons to ~200 keV and directs them to the quarter cryomodule. Since the electrons entering the cryomodule's first cavity are not fully relativistic, the energy gain is expected to be lower than optimal for this β =1 accelerating structure. A simple model consisting of two cavities was used to simulate the beam acceleration with ACE3P (an RF structure EM simulation code), GPT, and PARMELA (an electrodynamics simulations package) to estimate the energy gain [27-29]. Omega3P module of ACE3P was used to calculate the RF field and

output the field map for PARMELA and GPT for particle tracking. Figure 19 shows the one-dimensional normalized electric field map on axis for the corresponding cavities.

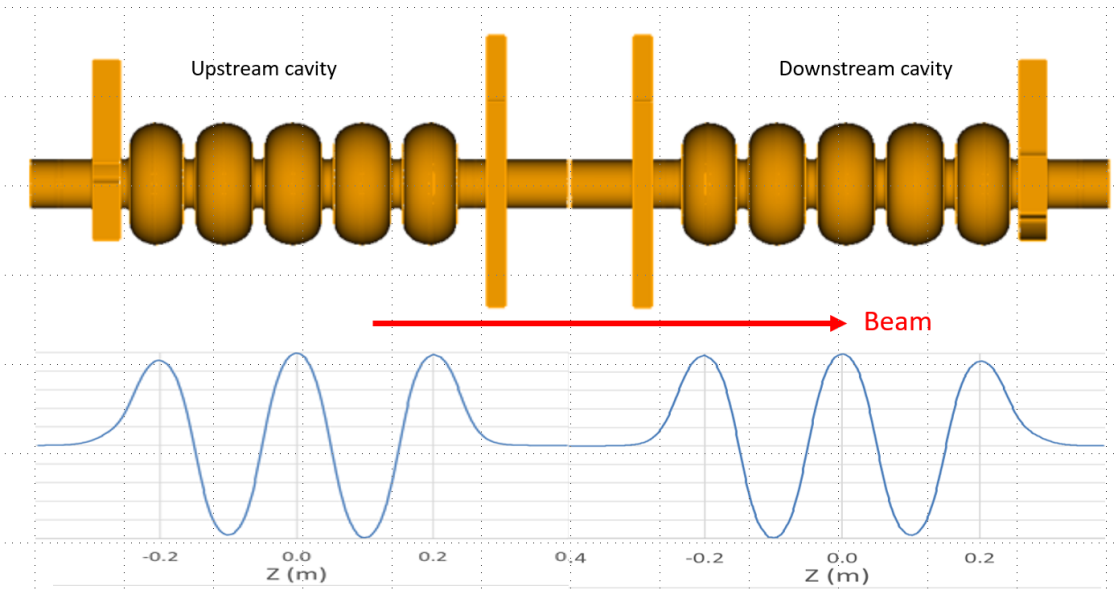

Figure 19: Model used to simulate beam acceleration through the pair of C75 five-cell cavities in the quarter cryomodule. Note the corresponding electric field map for each cavity.

Let's assume that each cavity in the cryomodule has a gradient of 10.13 MV/m. The incoming beam for the upstream cavity has an energy of 197.662 keV (β = 0.69). The incoming beam for the downstream cavity has an energy of 2.7 MeV (β = 0.99). Figure 20 shows the estimated energy gain as the beam travels through each cavity, depending on the RF phase. The variation in the accelerating gradient causes a shift in the phase of maximum energy gain in the upstream cavity; see Figure 21 (left). The estimated energy gain for the pair's first cavity, the upstream cavity, for different gradient reach is also shown in Figure 21 (right). The energy gain for cavity gradient less than 12 MV/m is linearly related to the E_{acc}; the ratio is 1/3. For a gradient of more than 12 MV/m, the energy gain is almost constant at ~4 MeV. Since the beam is already relativistic before entering the second cavity, the energy gain is linearly related to the E_{acc}, and the ratio is ½ as the cavity is 0.5 m in length. The total energy gain from the cryomodule can be estimated using equation (1).

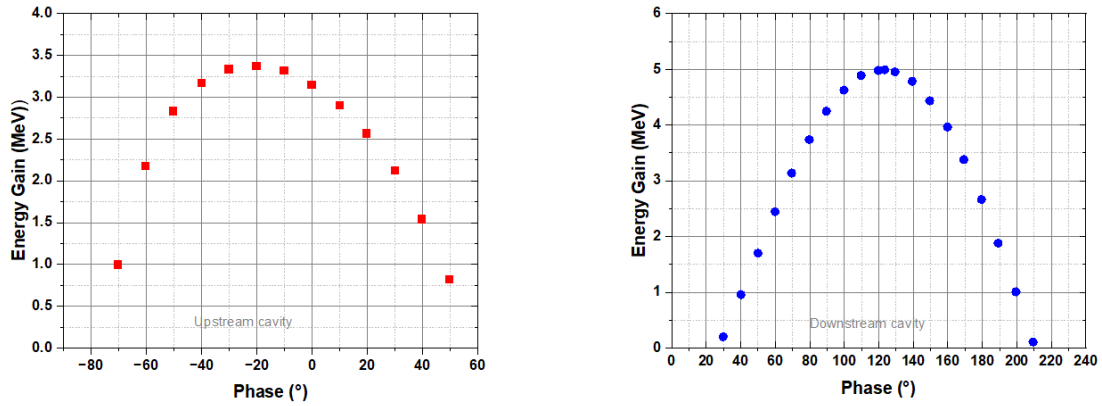

Figure 20: The energy gains vs. the phase (Φ) for the upstream cavity (left) and downstream cavity (right) for an accelerating gradient of 10.13 MV/m.

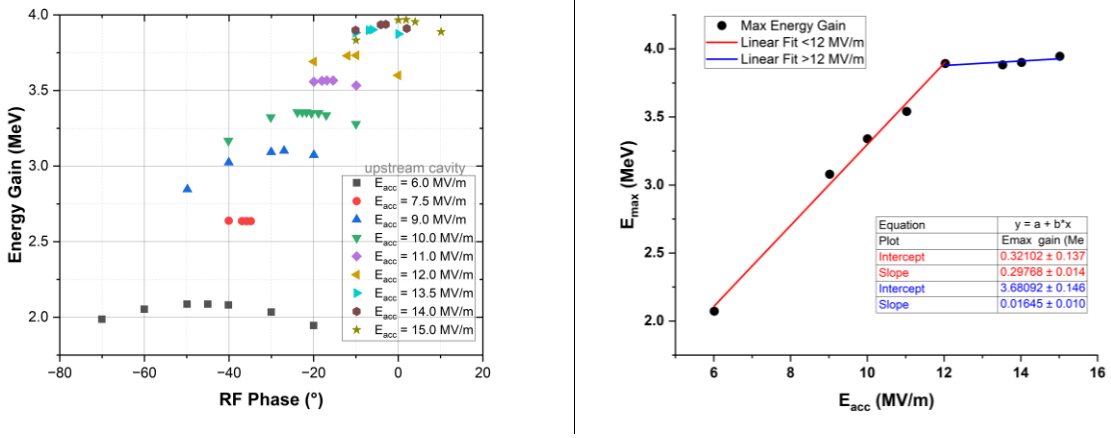

Figure 21: Phase scan of energy gain with various gradients for the upstream cavity (left). Energy gain as a function of the operational gradient of the upstream cavity (right). Note that the energy gain is almost constant at ~4 MeV for E_{acc}>12 MeV.

$$\boldsymbol{E_{gain}}(\text{MeV}) = \frac{1}{3}E_{acc,1}(\frac{\text{MV}}{\text{m}}) + \frac{1}{2}E_{acc,2}(\frac{MV}{m}) \qquad (1),$$

$E_{acc,1}$ and $E_{acc,2}$ are the gradient of upstream and downstream cavities in the quarter cryomodule, respectively. Based on the performance of Nb_3Sn cavities during the acceptance testing (Table 1), an energy gain of ~7.3 MeV is expected. Note that this estimation seems slightly higher than that previously reported by S. Pokhrel et al., in which a similar model consisting of two five-cell cavities was simulated with a General Particle Tracer [30].

Previously, a cw electron beam at the photo-injector was accelerated up to a total energy of 6.3 MeV at currents up to 80 μA using two 5-cell niobium cavities in the quarter-

cryomodule at 4 K in CEBAF [31]. Beam parameters under such cryomodule conditions were compared with similar measurements when the cryomodule was at 2 K. Beam parameters were very similar between 4 K and 2 K with any difference resulting from slightly different optics. With higher quality factors available in Nb_3Sn-coated cavities than those for Nb cavities, the cryogenic load is expected to be manageable to achieve the estimated energy gain.

6. Reference execution procedure for the beam test*

i. Cryomodule cooldown: The procedure will follow the typical cooldown protocol used for other cryomodules, except the cooldown parameters will need to be adjusted to achieve a cooldown rate of less than 30 K per hour for the initial cooldown from room temperature to 4.4 K while ensuring that the helium vessel pressure does not exceed 950 Torr. The temperature difference across the cavity pair must be strictly maintained below 0.3 K from 20 K to 10 K to ensure all parts cool uniformly below the transition temperature. Detailed protocol and requirements are available in the document, "Nb_3Sn cryomodule acceptance criteria", prepared for the cryomodule acceptance testing.

ii. Cryomodule performance validation: Following the first cooldown, the operational and maximum gradients, as well as the quality factors for each cavity at 4.4 K and 2.0 K, will be verified, as summarized in Table 2. The performance evaluation procedure follows the process outlined for the quarter cryomodule acceptance testing.

iii. Cavity Tuning: Cavity 5C75-RI-04, the downstream cavity, will be the only cavity to be tuned for the initial beam test. ~ 180 kHz tuning at 2.0 K is required to match the upstream cavity's frequency, 5C75-RI-NbSn01 (see Table 3).

iv. Thermal cycle: In case assuming cavity quenching occurs during performance validation and tuning resulting in quality factor degradation, the cryomodule shall be warmed up to 30 K and then uniformly cooled down to 2.0 K to recover the quality factors, as described in Step (i) above

v. Beam Acceleration at 2.0 K: beam acceleration in continuous wave mode at the set gradient of 3.0 MV/m in both cavities for stable operation for 1 h.

vi. Beam Acceleration at 4.4 K: beam acceleration in continuous wave mode at the set gradient of 3.0 MV/m in both cavities for stable operation for 1 h.

vii. Gradually raise the cavity set gradients (up to 12.6 MV/m for the upstream cavity and 7.5 MV/m for the downstream cavity) for stable operation for 1 hr.

Depending on whether the cavities quench, the cryomodule may require thermal cycling between the beam tests. The injection beam current may be varied for the beam acceleration at each temperature. The high-level objective of the first beam test is defined in [32]. A follow-up beam test will be planned, which will be informed by the outcome of the first beam test.

**These steps will be taken into account to develop a comprehensive beam test plan.*

References

[1] H. Padamsee, J. Knobloch and T. Hays, "RF Superconductivity for Accelerators" John Wiley & Sons," Inc., New York, pp. 199, 1998.

[2] R. L. Geng, G. V. Eremeev, H. Padamsee, and V. D. Shemelin, "High Gradient Studies for ILC with Single-Cell Re-Entrant Shape and Elliptical Shape Cavities made of Fine-Grain and Large-Grain Niobium," Proc. PAC07, Albuquerque, New Mexico, USA, WEPMS006 (2007)

[3] Furuta, F., Saito, K., Saeki, T., Inoue, H., Morozumi, Y., Higo, T., Higashi, Y., Matsumoto, H., Kazakov, S., Yamaoka, H. and Ueno, K.,, "Experimental Comparison at KEK of High Gradient Performance of Different Single Cell Superconducting Cavity Designs", in Proc. 10th European Particle Accelerator Conf. (EPAC'06), Edinburgh, UK, Jun. 2006, paper MOPLS084.

[4] A. Grassellino, A. Romanenko, D. Sergatskov, O. Melnychuk, Y. Trenikhina, A. Crawford, A. Rowe, M. Wong, T. Khabiboulline, and F. Barkov, "Nitrogen and argon doping of niobium for superconducting radio frequency cavities: A pathway to highly efficient accelerating structures," Supercond. Sci. Technol. 26, 102001 (2013).

[5] P. Dhakal, "Nitrogen doping and infusion in SRF cavities: A review," Phys. Open 5, 100034 (2020).

[6] D. Bafia Bafia, A. Grassellino, O. Melnychuk, A.Romanenko, Z.H. Sung, and J. Zasadzinski et al., "Gradients of 50 MV/m in TESLA shaped cavities via modified low temperature bake," Proc. 19th Int. Conf. on RF Superconductivity, Dresden, Germany, TUP061 (2019).

[7] B. Hillenbrand, H. Martens, H. Pfister, K. Schnitzke, and Y. Uzel, "Superconducting Nb_3Sn cavities with high microwave qualities," IEEE Trans. Magn., vol. 13, (1), pp. 491-495, 1977.

[8] G. Müller, H. Piel, J. Pouryamout, P. Boccard, and P. Kneisel, "Status and prospects of Nb_3Sn cavities for superconducting linacs," in Proceedings of the Workshop on Thin Film Coating Methods for Superconducting Accelerating Cavities, 2000.

[9]P. Kneisel, D. Mansen, G. Mueller, H. Piel, J. Pouryamout, and R. Roeth, "Nb_3Sn Layers on High-Purity Nb Cavities with Very High Quality Factors and Accelerating Gradients", in Proc. EPAC'96, Sitges, Spain, Jun. 1996, paper WEP002L

[10] S. Posen, D.L. Hall, and M. Liepe, “Proof-of-principle demonstration of Nb_3Sn superconducting radiofrequency cavities for high Q0 applications,” Appl. Phys. Lett. 106, 082601 (2015).

[11] U. Pudasaini, C. E. Reece, and J. K. Tiskumara, “Managing Sn-Supply to Tune Surface Characteristics of Vapor-Diffusion Coating of Nb_3Sn”, presented at the SRF'21, East Lansing, MI, USA, Jun.-Jul. 2021, doi:10.18429/JACoW-SRF2021-TUPTEV013.

[12] R.D. Porter, T. Arias, P. Cueva, D. L. Hall, M. Liepe, J. T. Maniscalco, D. A. Muller, and N. Sitaraman, “Next Generation Nb_3Sn Cavities for Linear Accelerators,” Proc. LINAC’18, Beijing, China (2018).

[13] S. Posen, J. Lee, D.N. Seidman, A. Romanenko, B. Tennis. O. S. Melnychuk, D.A.Sergatskov. “Advances in Nb_3Sn superconducting radiofrequency cavities towards first practical accelerator applications” Superconductor Science and Technology. 2021 Jan 11;34(2):025007.

[14] G. Eremeev., W. Clemens, K. Macha, C. E. Reece, A. M. Valente-Feliciano, S. Williams, U. Pudasaini, and M. Kelley. "Nb_3Sn multicell cavity coating system at Jefferson Lab." Review of Scientific Instruments 91, no. 7 (2020): 073911.

[15]R.C. Dhuley. S. Posen, M. I. Geelhoed, O. Prokofiev, and J. C. T. Thangaraj. "First demonstration of a cryocooler conduction cooled superconducting radiofrequency cavity operating at practical cw accelerating gradients." Superconductor Science and Technology 33, no. 6 (2020): 06LT01.

[16] G. Ciovati, G. Cheng, U. Pudasaini, and R. A. Rimmer. "Multi-metallic conduction cooled superconducting radio-frequency cavity with high thermal stability." Superconductor Science and Technology 33, no. 7 (2020): 07LT01.

[17] G. Ciovati et al. "Development of a prototype superconducting radio-frequency cavity for conduction-cooled accelerators." Physical Review Accelerators and Beams 26.4 (2023): 044701.

[18] N. A. Stilin et al. "RF and thermal studies on conduction cooled Nb_3Sn SRF cavity." Engineering Research Express 5.2 (2023): 025078.

[19] R.C. Dhuley et al., “Design of a medium energy, high average power superconducting e-beam accelerator for environmental applications,” arXiv:2112.09233 (2021).

[20] G. Ciovati et. al.,, “Design of a cw, low-energy, high-power superconducting linac for environmental applications,” Phys. Rev. Accel. Beams 21, 091601 (2018).

[21] Z. Yang et al. "Stable Acceleration of a LHe-Free Nb_3Sn demo SRF e-linac Based on Conduction Cooling." arXiv preprint arXiv:2404.09187 (2024).

[22] M. W. Bruker et al. “Operational Experience of the New Booster Cryomodule at the Upgraded Injector Test Facility”. No. JLAB-ACC-22-3675; DOE/OR/23177-5556. Thomas Jefferson National Accelerator Facility (TJNAF), Newport News, VA (United States), 2022.

[23] C. Leemann, “CEBAF design overview and project status”, in Third Workshop on RF Superconductivity, edited by K.W. Sheperd (1987)

[24] U. Pudasaini, G. V. Eremeev, M. J. Kelley, and C. E. Reece, "Recent Developments of Nb?Sn at Jefferson Lab for SRF Accelerator Application", in *Proc. NAPAC'19*, Lansing, MI, USA, Sep. 2019, pp. 713-716. doi:10.18429/JACoW-NAPAC2019-WEPLM5

[25] G. V. Eremeev *et al.*, "Preservation of the High Quality Factor and Accelerating Gradient of Nb_3Sn-Coated Cavity During Pair Assembly", in *Proc. SRF'23*, Grand Rapids, MI, USA, Jun. 2023, paper TUPTB010, pp. 405-409.

[26] S. Posen et al., "Nb?Sn at Fermilab: Exploring Performance", in Proc. SRF'19, Dresden, Germany, Jun.-Jul. 2019, pp. 818-822. doi:10.18429/JACoW-SRF2019-THFUB1

[27] https://confluence.slac.stanford.edu/display/AdvComp/ACE3P+-+Advanced +Computational +Electromagnetic+Simulation+Suite

[28] https://www.pulsar.nl/index.html

[29] L. M. Young and J. Billen, "The Particle Tracking Code PARMELA", in Proc. PAC'03, Portland, OR, USA, May 2003, paper FPAG029, pp. 3521-3523.

[30] S. Pokharel, A. S. Hofler, and G. A. Krafft, "Modeling a Nb_3Sn Cryounit in GPT at UITF", in Proc. IPAC'22, Bangkok, Thailand, Jun. 2022, pp. 576-579. doi:10.18429/JACoW-IPAC2022-MOPOTK051

[31] G. V. Eremeev *et al.*, "4 K SRF Operation of the 10 MeV CEBAF Photo-Injector", in *Proc. LINAC'16*, East Lansing, MI, USA, Sep. 2016, pp. 155-157. doi:10.18429/JACoW-LINAC2016-MOPLR010

[32] R. Geng, U. Pudasaini, "Nb_3Sn Quarter Cryomodule (Gray Enid I) First Beam Test: Objective, Key Metrics, and Interface Parameters". JLAB-TN-24-051.